Minimal Fokker-Planck Theory for the Thermalization of Mesoscopic Subsystems

Igor Tikhonenkov,[1] Amichay Vardi,[1] James R. Anglin,[2] and Doron Cohen[3]
[1]Department of Chemistry, Ben Gurion University of the Negev, Beer Sheva 84105, Israel
[2]OPTIMAS Research Center and Fachbereich Physik, Technische Universität Kaiserslautern, D-67653 Kaiserslautern, Germany
[3]Department of Physics, Ben Gurion University of the Negev, Beer Sheva 84105, Israel
(Received 10 October 2012; published 30 January 2013)

We explore a minimal paradigm for thermalization, consisting of two weakly coupled, low dimensional, nonintegrable subsystems. As demonstrated for Bose-Hubbard trimers, chaotic ergodicity results in a diffusive response of each subsystem, insensitive to the details of the drive exerted on it by the other. This supports the hypothesis that thermalization can be described by a Fokker-Planck equation. We also observe, however, that Levy-flight type anomalies may arise in mesoscopic systems, due to the wide range of time scales that characterize 'sticky' dynamics.

DOI: 10.1103/PhysRevLett.110.050401 PACS numbers: 05.30.Jp, 03.65.−w, 05.45.Mt, 05.70.Ln

The emergence of irreversibility from reversible Hamiltonian mechanics remains an open fundamental question, even after a century of effort. Recent advances in computational as well as experimental technique may at last bring answers within reach. The biggest challenge of this quest is the sheer technical difficulty of solving the Hamiltonian evolution of quantum many-body systems, even when they are quite small and isolated. In this Letter, we propose to leap over a significant barrier of understanding, by using Hamiltonian results from a tractable but nontrivial system, to support an extension of an established phenomenological theory, into a substantially more challenging regime. The result we thereby derive is a simple theory that can then both guide, and be tested by, subsequent numerical investigations, as well as currently feasible experiments.

We address the thermalization of two nonlinear Hamiltonian subsystems that are weakly coupled together, where the combined system is isolated and undriven. The equilibration of such subsystems is postulated in the zeroth law of thermodynamics, reflecting the assumption that microscopic dynamics is unobservably fast, while slower macroscopic dynamics remains nontrivial. Accordingly, weakly coupled subsystems, each having strong internal interactions, provide the minimal paradigm for the emergence of thermodynamics from closed-system mechanics.

Following the Fermi-Pasta-Ulam numerical experiment, most studies of dynamical equilibration have historically focused on large, extended systems [1,2], where the treatment of even one strongly interacting system is quite impossible in microscopic detail. With experimental access to controlled mesoscopic systems, attention has more recently been drawn to thermalization phenomena in small systems, taking into account dynamical chaos [3,4] and quantum effects [5–8]. The traditional analysis of thermalization has nonetheless largely remained within the assumptions inherited from the macroscopic problem. It is common to assume that at least one of the two coupled systems is "big", and hence, can be drastically approximated, either as a phenomenologically described reservoir, or as a time-dependent external parameter. The present Letter is motivated by the realization that the study of isolated thermalization of two subsystems is no longer so unthinkably intractable. It is merely extremely difficult. Our proposal is to leverage our understanding of driven chaotic systems to overcome this difficulty, by viewing each subsystem as driving the other.

The statistical approach.—The statistical description of driven chaotic systems by means of a Fokker-Planck equation (FPE) for their energy distribution [9–14] is based on the ergodic adiabatic theorem [15]. Quantum and classical systems can be embraced in a unified notation by writing the energy ε as a function of the phase space volume n of the constant-energy hypersurface. The density of states is $g(\varepsilon) = dn/d\varepsilon$ and the microcanonical inverse temperature is $\beta(\varepsilon) = d\ln(g)/d\varepsilon$. Upon quantization, the Wigner-Weyl formalism implies that n corresponds to the discrete index of the energy levels ε_n, and if these levels are dense enough, they can be approximated as a quasicontinuum. One then makes a coarse-grained description of the slow evolution of the system, and derives an FPE to describe the evolution of the time-dependent energy probability distribution $\rho(\varepsilon, t)$.

FPE for a driven system.—If a chaotic system is driven weakly, its energy changes slowly, and $\rho(\varepsilon, t)$ obeys a probability-conserving FPE, whose diffusion term has a coefficient D, proportional to the strength of the driving [9–11,14]. By Liouville's theorem, a distribution $\rho(\varepsilon) \propto g(\epsilon)$ should be a time-independent solution of the FPE. Hence, it is deduced that the drift term in the FPE is universally related to D, and the complete phenomenological equation is established.

FPE for coupled subsystems.—We now extend the single-system FPE phenomenology [9–11] to the case of thermalization of *two* subsystems. Each subsystem ($i = 1, 2$) is characterized by its density of states $g_i(\varepsilon_i)$

and by its microcanonical inverse temperature β_i. Thanks to conservation of energy the thermalization is within subspaces of constant energy $\varepsilon_1(n_1) + \varepsilon_2(n_2) = \mathcal{E}$. Accordingly, we set $\varepsilon_1 = \varepsilon$, and $\varepsilon_2 = \mathcal{E} - \varepsilon$, and construct an FPE for the probability density $\rho(\varepsilon, t)$ that describes how the energy is divided between the two subsystems.

It again follows from Liouville's theorem that an ergodic distribution, $\rho(\varepsilon) \propto g(\varepsilon) \equiv g_1(\varepsilon)g_2(\mathcal{E} - \varepsilon)$, should be a stationary solution. This fixes the form of the FPE, and implies the functional form of the drift term:

$$\frac{\partial \rho}{\partial t} = \frac{\partial}{\partial \varepsilon}\left[g(\varepsilon)D(\varepsilon)\frac{\partial}{\partial \varepsilon}\left(\frac{1}{g(\varepsilon)}\rho\right)\right] \tag{1}$$

$$= -\frac{\partial}{\partial \varepsilon}\left(A(\varepsilon)\rho - \frac{\partial}{\partial \varepsilon}[D(\varepsilon)\rho]\right). \tag{2}$$

It is important to notice that the diffusion coefficient D may depend on ε. The optional way, Eq. (2), of writing this FPE demonstrates that the 'drift velocity' A is related to the diffusion as follows:

$$A(\varepsilon) = \partial_\varepsilon D + (\beta_1 - \beta_2)D. \tag{3}$$

To see more clearly the connection of Eq. (3) with traditional thermodynamics, assume that each of the subsystems is prepared independently in a canonical state, with temperature T_i, such that $g_i(\varepsilon_i)\exp(-\varepsilon_i/T_i)$ describes its energy distribution. Integrating both sides of Eq. (3) with this probability measure, and integrating by parts the first term on the right, one obtains [4] a mesoscopic Einstein relation, like those previously derived [16,17] using master-equation or fluctuation-theorem approaches:

$$\frac{d}{dt}\langle \varepsilon \rangle = \langle A(\varepsilon) \rangle = \left(\frac{1}{T_1} - \frac{1}{T_2}\right)\langle D \rangle. \tag{4}$$

This result offers insight into the distinct behaviors of microcanonical energy fluctuations and canonical averages. The canonical version Eq. (4) implies that energy always flows from the higher to the lower canonical temperature, but the more general mesoscopic version Eq. (3) implies that energy flow is not necessarily from the higher to the lower microcanonical temperature and may depend on the functional form of $D(\varepsilon)$. This is not in contradiction with the zeroth law of thermodynamics: energy fluctuates between finite systems in equilibrium such that their average microcanonical temperatures need not be equal. The ergodic solution $\rho \propto g(\varepsilon)$ around which Eq. (1) has been constructed implies only that the most probable ε is the one for which $\beta_1(\varepsilon) = \beta_2(\mathcal{E} - \varepsilon)$.

Fluctuation-dissipation phenomenology.—The derivation of Eq. (1) is phenomenological but based on simple assumptions that can be tested. Since these include weak coupling, it is further consistent to compute D using the Kubo formula. Writing the interaction as $\mathcal{H} = Q^{(1)}Q^{(2)}$, and defining $\tilde{S}^{(i)}(\omega)$ as the power spectrum of the fluctuating variable $Q^{(i)}(t)$, it reads [18]

$$D = \int_0^\infty \frac{d\omega}{2\pi}\omega^2 \tilde{S}^{(1)}(\omega)\tilde{S}^{(2)}(\omega). \tag{5}$$

With this addition, the FPE phenomenology provides a generalized fluctuation-dissipation relation that connects the systematic energy flow between the subsystems with the intensity of the fluctuations.

Reasoning.—When two undriven subsystems are coupled to each other, the effect of one subsystem (call it "agent") on the other (call it "system") is like that of driving. For the purpose of obtaining Eq. (1), we have assumed that the interaction results in diffusion that can be calculated using Eq. (5). Future studies of coupled systems must test this assumption in full, but one key point remains to be established with regard to the driven single-subsystem dynamics: The agent-system interaction will typically couple many quantum levels, even if it is weak in classical terms. In such strongly nonadiabatic circumstances, energy diffusion, and the applicability of Eq. (5), have not been demonstrated [4]. Below, we complete this Letter by a numerical demonstration that highlights the role of chaos in obtaining diffusive dynamics for a driven subsystem, supporting the feasibility of the above reasoning for experimentally relevant systems.

Testing ground.—Few-mode Bose-Hubbard systems are a promising testing ground, since they are experimentally accessible and highly tunable [19], and theoretically tractable by a wide range of techniques. Since boson number is conserved, their Hilbert spaces are of finite dimension, and yet their classical dynamics can be nonintegrable. The smallest Bose-Hubbard system admitting chaos without external driving is the three-mode *trimer* [20–26], described by the Bose-Hubbard Hamiltonian (BHH):

$$\mathcal{H} = \frac{K}{2}\sum_{i=1,2}(a_i^\dagger a_0 + a_0^\dagger a_i) + \frac{U}{2}\sum_{i=0,1,2} a_i^\dagger a_i^\dagger a_i a_i, \tag{6}$$

Here, $i = 0, 1, 2$ label the three modes, a_i and $a_i^\dagger$ are canonical destruction and creation operators in second quantization, K is the hopping frequency, and U is the on site interaction. The Hamiltonian $\mathcal{H}$ commutes with the total particle number $\mathcal{N} = \sum_i a_i^\dagger a_i$, and hence, without loss of generality, we regard $\mathcal{N}$ as having a definite value N. Driving is then implemented by setting $K = K_0 + K_d\sin(\Omega t)$. Consequently, the total Hamiltonian has the structure $\mathcal{H}_0 + f(t)W$, where the perturbation operator W is identified as the first sum in Eq. (6) and the driving field is $f(t) = (K_d/2)\sin(\Omega t)$.

Chaoticity.—The underlying classical dynamics is defined [4] by replacing the operators a_i in the Heisenberg equations of motion [27] with complex c numbers $\sqrt{n_i}e^{i\varphi_i}$. In the absence of driving, up to trivial rescaling, the classical equations depend only on the single dimensionless parameter $u = NU/K_0$. The chaoticity of the motion that is generated by $\mathcal{H}_0$ is reflected in the local level statistics and can be quantified by the Brody

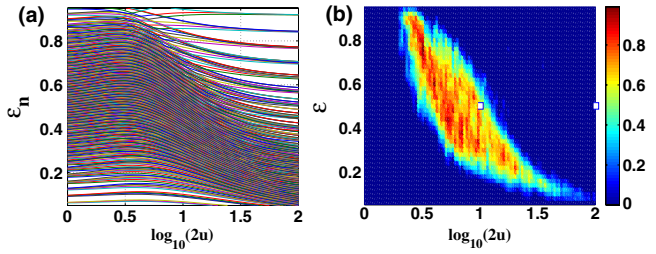

FIG. 1 (color online). The energy spectrum of the unperturbed BHH. In panel (a), the scaled eigenenergies ε_n of $\mathcal{H}_0$ are plotted vs the scaled interaction parameter, u, for $N = 35$ particles. The level spacing statistics is characterized by the Brody parameter $(0 < q < 1)$, which is displayed in panel (b) for a system with $N = 120$ particles. In the energy range where the motion is chaotic, $q \sim 1$. Square symbols indicate the preparations that were used for the simulations in Fig. 2.

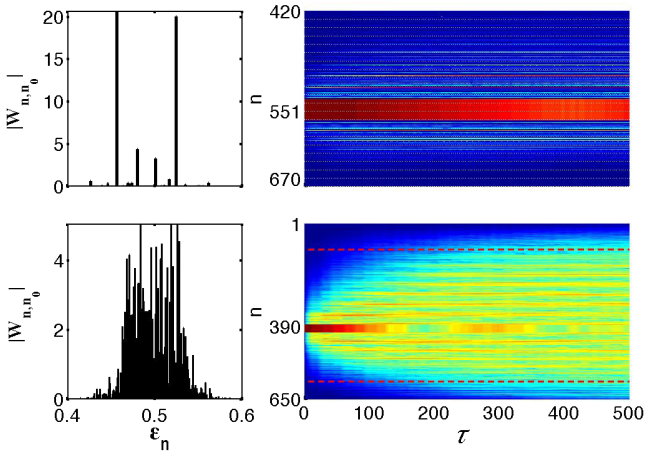

FIG. 2 (color online). The quantum probability distribution $p_n(t)$ for representative simulations is imaged as a function of time (right). The short-time energy-spreading profile is determined by the perturbation matrix $|W_{n,n_0}|^2$ (left). The number of particles is $N = 50$. The upper set is for $u = 50$ and the lower is for $u = 5$. The strength of the driving is $K_d/K_0 = 0.1$. For the time axis, we use dimensionless units, $\tau = (E_{\max} - E_0)t/\hbar$, and the scaled driving frequency in both simulations is $\Omega \approx 0.03$. The image of the initial level is vertically zoomed and it has the energy $\varepsilon \approx 0.5$. The boundaries of the chaotic sea in the lower image are indicated by the horizontal dashed lines.

parameter $0 < q < 1$ [28], such that $q = 0$ indicates a Poissonian level-spacing distribution (characteristic of integrable dynamics), while higher values indicate the approach to Wigner level-spacing distribution (indicating chaotic dynamics).

Figure 1(a) displays the spectrum ε_n, obtained by numerical diagonalization of $\mathcal{H}_0$, as a function of u. For graphical presentation, we shift and scale the energy spectrum, for each u, into the same range $\varepsilon \in [0, 1]$, such that $\varepsilon = 0$ and $\varepsilon = 1$ are the ground energy E_0 and the highest energy $E_{\max}$, respectively. By plotting q vs (u, ε), as in Fig. 1(b), we can identify the ε range within which the motion is chaotic at any given value of u. See Ref. [4] for technical details. We have verified the implied chaoticity by plotting representative classical Poincaré cross sections.

In the numerical simulations, we consider an $N = 50$ particle system with two representative values of u. The case $u = 5$, for which there is a wide chaotic range $0.2 < \varepsilon < 0.6$, is contrasted with $u = 50$, for which the motion is globally quasi-integrable due to self-trapping.

Energy diffusion.—In the absence of driving, the energy is a constant of motion. Driving induces transitions between energy eigenstates, leading to a time-dependent spread in energy $\Delta\varepsilon(t)$. This dispersion is defined as the square root of the variance $\mathrm{Var}(\epsilon_n)$ that is associated with the probability distribution

$$p_n(t) = |\langle \varepsilon_n | \Psi(t) \rangle|^2. \tag{7}$$

In Fig. 2, we plot the time evolution of the quantum energy distribution $p_n(t)$ in response to driving that is quantum mechanically large (many levels are mixed) but classically small ($K_d \ll K_0$). We contrast the response in the chaotic ($u = 5$) and in the quasi-integrable ($u = 50$) regimes. Dramatic differences are observed. In both cases, the energy distribution in the very early stages of the evolution reflects the band profile of the perturbation matrix W_{n,n_0}, where n_0 is the initial level, as expected from time-dependent first-order perturbation theory. Later in the evolution, higher orders of perturbation theory dominate. This leads in the quasi-integrable case to Rabi-like oscillations that have no relation to the classical dynamics. But in the chaotic regime, one observes that the driving is capable of inducing diffusive-like energy spreading. This diffusive spreading is restricted to the chaotic energy window and features remarkable correspondence with the classical simulation.

Linear response.—The diffusive energy spreading in the chaotic regime can be quantified by the time evolution of the energy variance. In Fig. 3, we plot the time evolution of $\Delta\varepsilon$ for both the chaotic and the integrable cases. In both cases, we compare the dispersion obtained under the classical equations of motion for the driven system, starting from a microcanonical ensemble, to that obtained from quantum evolution from an eigenstate with the same energy. As anticipated for diffusive energy spreading, we observe that in the chaotic regime $(\Delta\varepsilon)^2 \approx 2Dt$ with diffusion coefficient $D \propto K_d^2$, as assumed in the Kubo linear response formula Eq. (5).

In Fig. 4, we compare the diffusive energy distribution that is observed in Fig. 2, with the solution of the FPE Eq. (1), using the diffusion coefficient from Eq. (5), see Ref. [4] for technical details. The agreement is good, confirming that weakly driven chaotic quantum systems can indeed exhibit energy diffusion in regimes realistic for experimental Bose-Hubbard systems and solidifying the basis of our phenomenological argument for the FPE description of intersubsystem equilibration.

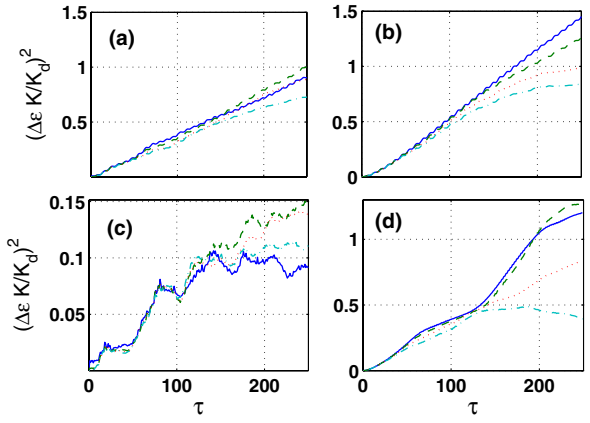

FIG. 3 (color online). The scaled variance as a function of the scaled time in the classical (left) and in the quantum (right) simulations. The value of the scaled interaction parameter is $u = 5$ (upper panels) and $u = 50$ (lower panels). Note the different scale of the vertical axis for the quantum vs classical simulations in panels (c) and (d). Clearly quantum-to-classical correspondence fails in the quasi-integrable regime. The values of K_d/K_0 are 0.025 (blue), 0.05 (green), 0.075 (red), and 0.1 (cyan). The driving frequency is as in Fig. 2.

Multiple time scales.—Having established quite good quantum-to-classical correspondence in the chaotic regime, one wonders whether classical dynamics may indicate features that go beyond simple energy diffusion. Figure 5 illustrates the *classical* time dependence of $\varepsilon(t)$ and characterizes it by its average value and dispersion. Since the phase space has dimension greater than two, the possibility of Arnold diffusion guarantees that the motion is ergodic within the chaotic sea. This means that we can regard different trajectory segments as uncorrelated pieces of the same infinite time trajectory. If we had ergodic motion with a well-defined characteristic time, all the segments would have the same average and dispersion. But this is not what we see: the segments have large variation in their dispersion, since they do not uniformly fill the whole chaotic region. Rather, the trajectories contain episodes with long dwell times within some sticky regions in phase space, whose existence has been confirmed with a Poincaré section, see Ref. [4]. If we had an unlimited computation power, obviously the expectation is to have coincidence of all the points in the right panel of Fig. 5. But in practice, we can address only finite time intervals, and therefore, the points are scattered over a large range.

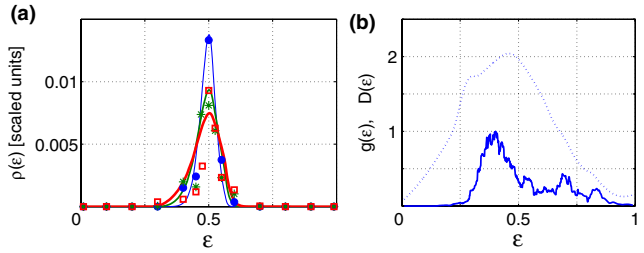

FIG. 4 (color online). (a) The evolving spreading profile $\rho(E)$, referring to the simulation that has been imaged in the lower panel of Fig. 2. The solid lines (calculation) and the associated symbols (simulation) are for $\tau = 149$ (narrower), and $\tau = 299$ (wider), and $\tau = 448$ (widest). The lines are based on the numerical solution of Eq. (1). (b) The density of states $g(E)$ (dotted line) and the diffusion coefficient $D(E)$ (solid line) were deduced from the diagonalization of the BHH and Eq. (5), see Ref. [4] for technical details.

Discussion.—We have considered few-mode Bose-Hubbard systems as tunably chaotic systems, which in chaotic regimes respond generically to weak driving with energy diffusion at a rate proportional to the square of the driving strength, K_d^2. Consequently, we deduce that the thermalization of coupled Bose-Hubbard subsystems can plausibly be described by a phenomenological FPE, namely Eq. (1).

We have also obtained some insight on how such phenomenological theories are affected by taking into account specific semiclassical features of the dynamics. A small subsystem can exhibit multiple time scales in its equilibration, because its phase space contains sticky regions with long dwell times. In principle, this may give rise to non-Gaussian features, and Lévy-flight related deviations from strict diffusive behavior. Even if these possibilities do not manifest strongly in energy spreading of small, driven systems because the explored phase space volume is small, they may perhaps become important in multicomponent composite systems. It would be important to recognize, then, in interpreting experiments or simulations intended to test Eq. (1), that some deviations from its diffusive assumptions may not represent errors in its depiction of the mesoscopic onset of irreversibility, but only the fading traces of microscopic behavior.

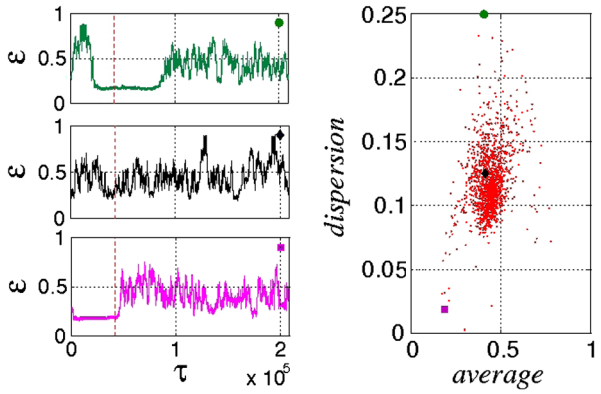

FIG. 5 (color online). On the left, the scaled energy $\varepsilon(t)$ as a function of time is plotted for a few representative trajectories. The right panel displays the average value and the dispersion of ε within the time interval $0 < \tau < 40000$, for the representative trajectories (symbols), as well as for many other trajectories (points). Low dispersion values reflect the finite probability to encounter sticky motion. The parameters are the same as in the lower panel of Fig. 2, with initial points that have the energy $\varepsilon = 0.3$.

This research was supported by the Israel Science Foundation (Grants No. 346/11 and No. 29/11) and by the United States-Israel Binational Science Foundation (BSF).

[1] J.-P. Eckmann, C.-A. Pillet, and L. Rey-Bellet, Commun. Math. Phys. **201**, 657 (1999).
[2] M. C. Zheng, F. M. Ellis, T. Kottos, R. Fleischmann, T. Geisel, and T. Prosen, Phys. Rev. E **84**, 021119 (2011).
[3] J. R. Dorfman, *An Introduction to Chaos in Nonequilibrium Statistical Mechanics* (Cambridge University Press, Cambridge, 1999).
[4] See Supplemental Material at http://link.aps.org/supplemental/10.1103/PhysRevLett.110.050401 for a more detailed discussion regarding the role of chaos; the derivation of Eq. (4); the semiclassical form of the trimer Hamiltonian; the calculation of the Brody parameter in Fig. 1; the calculation of the diffusion coefficient in Fig. 4; and representative Poincaré sections that are related to Fig. 5.
[5] M. Srednicki, Phys. Rev. E **50**, 888 (1994).
[6] A. C. Cassidy, D. Mason, V. Dunjko, and M. Olshanii, Phys. Rev. Lett. **102**, 025302 (2009).
[7] M. Rigol, V. Dunjko, and M. Olshanii, Nature (London) **452**, 854 (2008).
[8] C. Ates, J. P. Garrahan, and I. Lesanovsky, Phys. Rev. Lett. **108**, 110603 (2012).
[9] M. Wilkinson, J. Phys. A **21**, 4021 (1988).
[10] C. Jarzynski, Phys. Rev. E **48**, 4340 (1993); Phys. Rev. Lett. **74**, 2937 (1995).
[11] D. Cohen, Ann. Phys. (N.Y.) **283**, 175 (2000).
[12] M. Wilkinson and E. J. Austin, J. Phys. A **28**, 2277 (1995).
[13] D. Cohen, Phys. Rev. Lett. **82**, 4951 (1999); D. Cohen and T. Kottos, Phys. Rev. Lett. **85**, 4839 (2000).
[14] G. Bunin, L. D'Alessio, Y. Kafri, and A. Polkovnikov, Nat. Phys. **7**, 913 (2011).
[15] E. Ott, Phys. Rev. Lett. **42**, 1628 (1979); R. Brown, E. Ott, and C. Grebogi, Phys. Rev. Lett. **59**, 1173 (1987); J. Stat. Phys. **49**, 511 (1987).
[16] For a simple derivation based on a master equation approach, see D. Hurowitz and D. Cohen, Europhys. Lett. **93**, 60 002 (2011).
[17] For a recent derivation based on the nonequilibrium fluctuation theorem, see G. Bunin and Y. Kafri, arXiv:1202.5053.
[18] For a recent pedagogical presentation, see D. Cohen, Phys. Scr. **T151**, 014035 (2012) and further references within.
[19] O. Morsch and M. Oberthaler, Rev. Mod. Phys. **78**, 179 (2006); I. Bloch, J. Dalibard, and W. Zwerger, Rev. Mod. Phys. **80**, 885 (2008).
[20] K. Nemoto, C. A. Holmes, G. J. Milburn, and W. J. Munro, Phys. Rev. A **63**, 013604 (2000).
[21] R. Franzosi and V. Penna, Phys. Rev. A **65**, 013601 (2001).
[22] M. Hiller, T. Kottos, and T. Geisel, Phys. Rev. A **73**, 061604(R) (2006).
[23] M. Hiller, T. Kottos, and T. Geisel, Phys. Rev. A **79**, 023621 (2009).
[24] E. M. Graefe, H. J. Korsch, and D. Witthaut, Phys. Rev. A **73**, 013617 (2006).
[25] T. F. Viscondi and K. Furuya, J. Phys. A **44**, 175301 (2011).
[26] P. Jason, M. Johansson, and K. Kirr, Phys. Rev. E **86**, 016214 (2012).
[27] P. Buonsante and V. Penna, J. Phys. A **41**, 175301 (2008).
[28] T. A. Brody, J. Flores, J. B. Fench, P. A. Mello, A. Pandey, and S. S. M. Wong, Rev. Mod. Phys. **53**, 385 (1981).